

# Protein tethered lipid bilayer: An alternative mimic of the biological membrane (Mini Review)

Renate L. C. Naumann<sup>a)</sup> and Wolfgang Knoll  
*Max Planck Institute for Polymer Research, 55128 Mainz, Germany*

(Received 23 January 2008; accepted 6 May 2008; published 11 July 2008)

An overview is given about results obtained so far with an alternative concept of solid-supported tethered lipid bilayers for the functional incorporation of membrane proteins. The incorporated protein itself acts as the tethering molecule resulting in a versatile system where the protein determines the characteristics of submembraneous space. This architecture is achieved through a metal chelating surface, onto which histidine-tagged (his-tagged) membrane proteins are able to bind in a reversible manner. The tethered bilayer membrane is generated by substitution of protein bound detergent molecules with lipids using *in situ* dialysis or adsorption. Histidine-tagged cytochrome c oxidase is used as a model protein in this study. However, the system should be applicable to all recombinant membrane proteins bearing a terminal his tag. The system is particularly designed, among other surface-analytical techniques, for a combined application of electrochemical and vibrational spectroscopy measurements. © 2008 American Vacuum Society. [DOI: 10.1116/1.2936939]

## I. INTRODUCTION

Membrane proteins play a major role in every living cell. These proteins are the key factors in the cell's metabolism, for example, in cell-cell interaction, signal transduction, and transport of ions and nutrients. Due to this important function, they are a preferred target for pharmaceuticals (currently more than 60% of consumed drugs). Contrary to this fundamental role in biology, functional characterization of membrane proteins remains a challenge. To address this problem, a variety of biomimetic membrane systems have been developed such as solid-supported membranes,<sup>1</sup> polymer-supported membranes,<sup>2</sup> hybrid bilayer lipid membranes,<sup>3</sup> and tethered bilayer lipid membranes (tBLMs).<sup>4,5</sup> Advantages and disadvantages of these systems have been discussed in a recent review.<sup>6</sup> All of them provide the lipid environment required for the function of the protein. Polymer-supported membranes also provide a hydrophilic cushion separating the lipid bilayer from the metal or semiconductor support so as to overcome the strong hydrophobic interaction of the protein with the solid support which otherwise would lead to impairment of the function or even the denaturation of the protein. The hydrophilic polymer seems to be the ideal substitute of the intermembrane space considering the tendency of lipid vesicles to spread on hydrophilic surfaces such as glass or silicon to spontaneously form well ordered fluid lipid bilayers. Polymer-supported membranes have thus been widely used, mostly as a model system of the cell surface.<sup>6,7</sup> The use as a model system for ion transport studies, however, was less frequent. Many of these systems do not fulfill the requirement known from patch clamp techniques, the gigaseal, to separate the signal of the receptor from the leak current of the membrane. Highly insulating polymer-supported membranes have been prepared, though,

provided a very smooth surface of the hydrophilic polymer could be achieved.<sup>8</sup> There are, however, many more examples taking advantage of the tethering strategy applied to polymers and more often to oligomeric hydrophilic spacers attached to the hydrophilic head group of a lipid molecule. Monolayers of such compounds provide the highly hydrophobic surface known to promote the spreading of vesicles and the formation of highly insulating lipid bilayers while the tethering molecules provide an interstitial space separating the protein from the surface by an aqueous reservoir. Polymeric tethers seem to be of greater advantage compared to oligomeric ones, provided they form highly ordered monolayers.<sup>9</sup> Short tether molecules, however, are particularly useful when redox proteins are to be addressed by bio-electronic coupling to the electrode. The tether molecule then may serve a second purpose, namely, the electronic wiring of the redox centers of the protein to the electrode. This purpose would be hard to achieve by hydrophilic polymers. One of the most promising systems investigated in this context is the protein tethered bilayer lipid membrane (ptBLM),<sup>10-13</sup> designed for complex redox-active membrane proteins such as the cytochrome c oxidase (CcO) (Fig. 1). It is based on a nitrilotriacetic acid (NTA) functionalized surface which, after chelation with Ni<sup>2+</sup> ions, reversibly binds proteins genetically engineered with histidine (his) tags. A lipid bilayer is then reconstituted *in situ* around the bound proteins which may be electronically addressed via the Ni complex. Among the benefits of this strategy is the predefined orientation of the protein with respect to the surface. Unidirectional charge transfer processes such as electron transfer (ET) and proton transfer can be specifically investigated. Two opposite orientations of the protein were investigated, either with the cytochrome c binding site pointing away from the electrode surface<sup>10-12</sup> or directed toward the electrode,<sup>13-15</sup> simply by engineering the his tag on the C terminus of subunit (SU) I<sup>16</sup> or SU II,<sup>17</sup> respectively. An overview will be given about the

<sup>a)</sup>Electronic mail: naumannr@mpip-mainz.pg.de

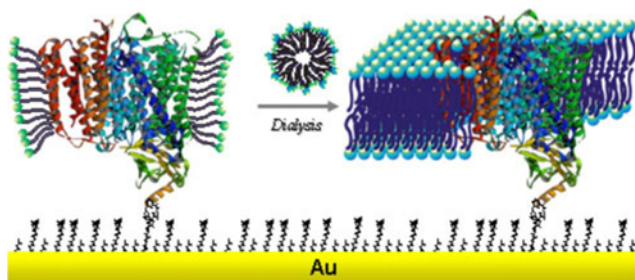


FIG. 1. Schematic representation of the reconstitution of CcO into a protein tethered bilayer lipid membrane. The protein is first attached to the surface of a chelator-modified gold film by the histidine tag genetically engineered to the protein. The lipid bilayer is then assembled around the protein by *in situ* dialysis of micelles made of a mixture of lipid and detergent.

results obtained so far with these two systems.

## II. MATERIALS AND METHODS

The materials and methods are described in detail in Refs. 10–16.

## III. ACTIVATION BY CYTOCHROME C

CcO from *P. denitrificans* with the his tag engineered to the C terminus of SU I was first immobilized in the orientation with the binding site of cytochrome c, the natural substrate of the CcO pointing away from the electrode.<sup>10</sup> Binding could be followed by surface-enhanced infrared reflection absorption (SEIRA) spectroscopy (Fig. 2).<sup>11</sup> Immobilization of the protein and the subsequent formation of the bilayer could also be observed by surface plasmon resonance (SPR) spectroscopy and by electrochemical impedance spectroscopy (EIS).<sup>12</sup> SPR allows to determine the optical thickness as a function of time (Fig. 3). From this recording, the time course of CcO binding was shown to be complete after 40 min, whereas *in situ* dialysis taking more than 20 h was usually done overnight. Approximate layer thicknesses (Table I) were obtained by fitting the parameters of the angle scans shown in the inset of Fig. 3. Protein bind-

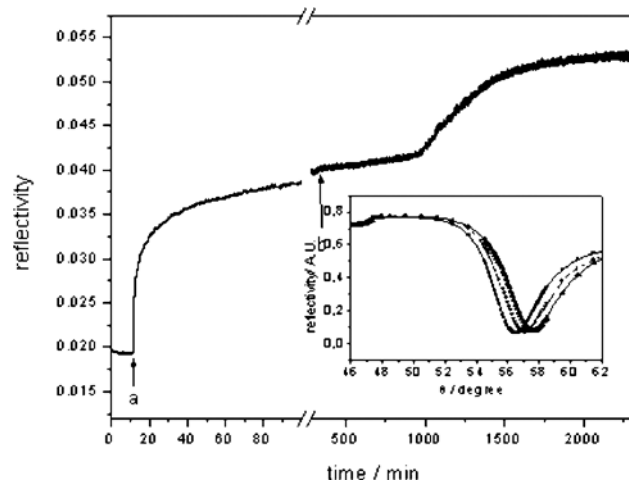


FIG. 3. SPR kinetic trace at a constant angle of incidence ( $55^\circ$ ). Binding of CcO is recorded after addition of the detergent-solubilized protein at (a); while the *in situ* dialysis is started at (b) by adding detergent-solubilized lipid and biobeads. Angle scans of the different layers are shown in the inset.

ing results in an increase in layer thickness of 8.7 nm, which corresponds to the height of the protein (9 nm) obtained from x-ray crystallography data. This indicates a relatively high surface coverage with the CcO. Impedance spectra were evaluated by fitting the parameter values of equivalent circuits to the measured impedance data before and after CcO binding and formation of the ptBLM [Fig. 4(a) and 4(b), respectively]. The equivalent circuit of the protein layer as well as the mixed protein-lipid membrane layer [Fig. 4(b)] was assumed to consist of one  $RC$  element represented by  $R_m$  and  $C_m$  ( $m$  stands for membrane) for the protein/detergent layer or the protein/lipid layer and a second  $RC$  element for the spacer layer ( $R_{sp}$  and  $CPE_{sp}$ ) in series with  $R_{ex}$ . Constant phase elements (CPEs) instead of pure capacitors are used because of the heterogeneity of the spacer layer. The parameter values obtained from the fitting procedure are shown in Table I. Reduced cytochrome c added to the bulk solution in the presence of oxygen activated the enzyme as seen in Fig.

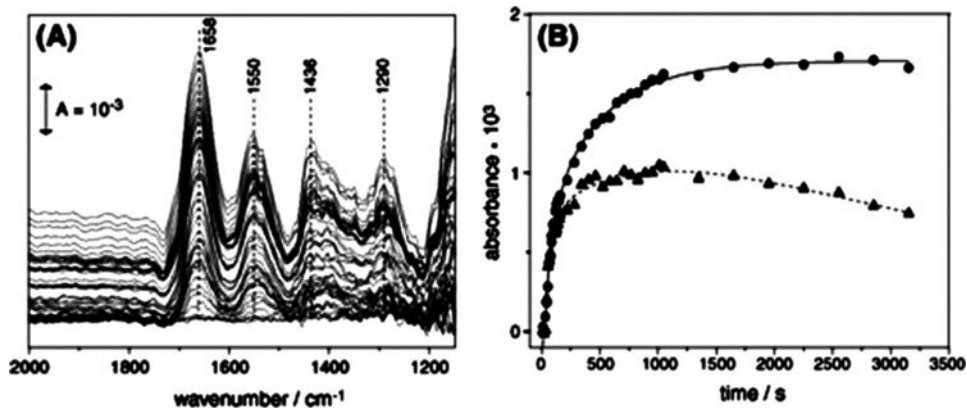


FIG. 2. (a) SEIRA spectra of cytochrome c oxidase from *P. denitrificans* adsorbed to the Ni-NTA modified Au surface via the affinity for the genetically introduced his tag attached to SU I. The rising bands indicate the binding of the protein to the surface (b) Adsorption kinetics of CcO on the Ni-NTA self-assembled monolayer/Au surface. The peak height of the amide II band at  $1550\text{ cm}^{-1}$  is plotted vs adsorption time. The filled circles represent the first adsorption of CcO, while the triangles represent the adsorption process of CcO after removing the previous CcO layer by imidazole.

TABLE I. Data obtained from CcO *P. denitrificans* engineered with the his tag attached to SU I. Electrical parameter values were obtained by fitting to the measured data of impedance spectra and thicknesses were obtained by fitting to the SPR angle scan plots.

	$R_m$ ( $\Omega \text{ cm}^2$ )	$C_m$ ( $\mu\text{F cm}^{-2}$ )	Layer thickness (SPR) (nm)
Ni-NTA layer			2.4
CcO layer before ptBLM formation	$(500 \pm 80) \times 10^3$	$12.1 \pm 2.8$	11.1
CcO layer after ptBLM formation	$(13 \pm 6) \times 10^6$	$7.1 \pm 0.5$	12.0
ptBLM after cyt c addition	$(550 \pm 90) \times 10^3$	$7.1 \pm 0.5$	n.d.

4(c). Proton transport across the membrane resulted in a decrease in the membrane resistance which could be abolished by cyanide, a potent inhibitor of CcO function.<sup>10,12</sup> This experiment indicates that the protein is immobilized on the surface in a functionally active state.

#### IV. DIRECT ELECTRON TRANSFER

CcO from *R. sphaeroides* engineered with a his tag on SU II (Ref. 17) was then immobilized into a ptBLM.<sup>13–15</sup> Under these conditions, the cytochrome c binding site, and hence also the first electron acceptor,  $\text{Cu}_A$ , is oriented toward the electrode surface. The cyclic voltammogram (CV), taken in a strictly anaerobic bathing solution, shows a single reduction peak at  $-274 \pm 7$  mV and a corresponding oxidation peak at  $-209 \pm 6$  mV [Fig. 5(a)] at low scan rates ( $<1 \text{ V s}^{-1}$ ). As the scan rate is increased to  $\sim 1 \text{ V s}^{-1}$ , the peak positions remain largely unchanged and the base-line-corrected current density increases linearly [inset of Fig. 5(a)], which is consistent with surface confined ET. The constant peak separation at scan rates  $<1 \text{ V s}^{-1}$  is observed only with the lipid membrane formed around the protein. Membrane formation was again checked by EIS and SPR (not shown). Finally, the apparent standard potential  $E_{\text{app}}^0$  was estimated by assuming symmetrical behavior of the redox system to be  $-242 \pm 7$  mV. This  $E_{\text{app}}^0$  is shifted  $\sim 450$  mV from the standard potential of 230 mV determined for the  $\text{Cu}_A$  center in isolated CcO.<sup>17</sup> This shift can be explained by the ET pathway to the enzyme via the Ni complex, taking into account the low standard potentials of chelated  $\text{Ni}^{2+}/\text{Ni}^+$  couples. The multistep ET to electron acceptors of very different standard potentials may result in a peak whose potential is located in between the single standard potentials, provided the first electron acceptor has a much lower standard potential compared to the following ones.

Strong evidence that ET observed by CV does take place directly into the enzyme was derived from Soret band excited surface-enhanced resonance Raman spectroscopy (SERRS) taken as a function of potential, under strictly anaerobic conditions (Fig. 6).<sup>13,14</sup> The maximum absorption feature of heme a and  $a_3$  sites of the protein, the so-called Soret band, is located at 410 nm.<sup>18,19</sup> Utilizing an excitation wavelength of 413 nm of the krypton laser, we take advantage of the selective resonant enhancement in the vibrational

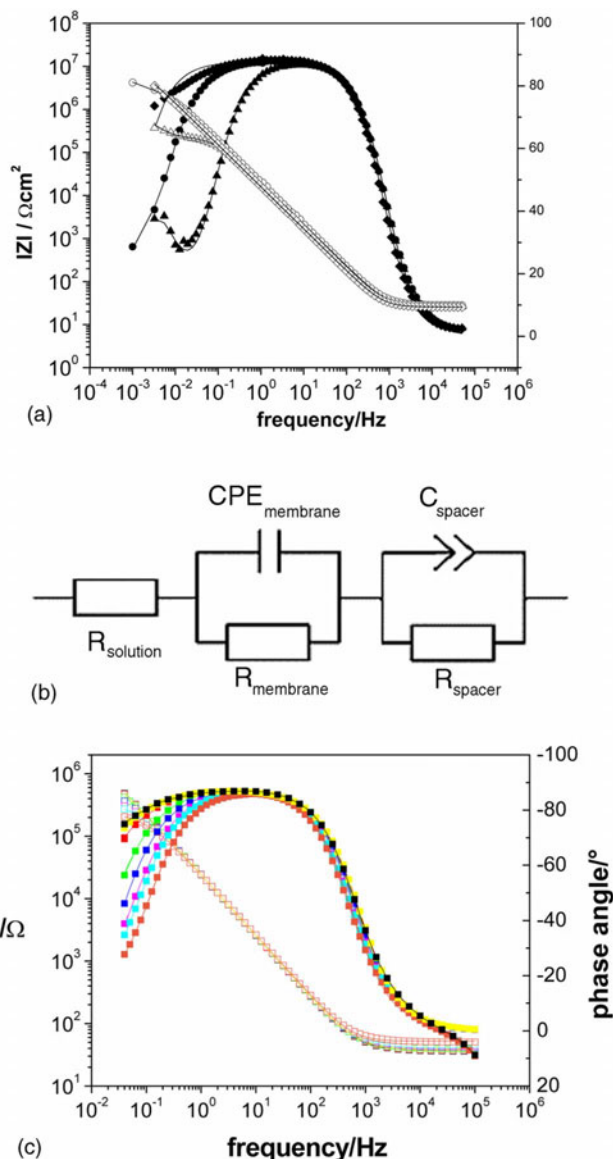


FIG. 4. Impedance spectra (Bode plots (a)), of the Ni-NTA modified surface before ( $\blacklozenge$ ) and after binding of CcO before ( $\bullet$ ) and after *in situ* dialysis to form the lipid bilayer around the protein ( $\blacktriangle$ ). Dotted lines represent experimental data, solid lines show the fitted curves using the equivalent circuits (b). Bode plots after adding increasing concentrations of cytochrome c from  $2.3 \times 10^{-4} \text{ M}$  to  $1.6 \times 10^{-3} \text{ M}$  (c).

modes of the heme sites. The characteristic marker band region ( $1300\text{--}1750 \text{ cm}^{-1}$ ) is very sensitive to the integrity of the enzyme and provides information on the redox state, ligation, spin, and coordination state of the heme a/ $a_3$  structure. The bands at  $1358$  and  $1370 \text{ cm}^{-1}$  originate from the  $\nu_4$  modes of both hemes in the reduced ( $-350$  mV) and oxidized states ( $-150$  mV), respectively.<sup>14,15</sup> These findings demonstrate a gradual transition of the redox state as well as the coordination and spin state of both heme centers in the potential range between  $-150$  and  $-350$  mV, in agreement with the CV data (Fig. 5).

Since the SERRS experiment is particularly designed for a selective resonance enhancement in the heme structure, the

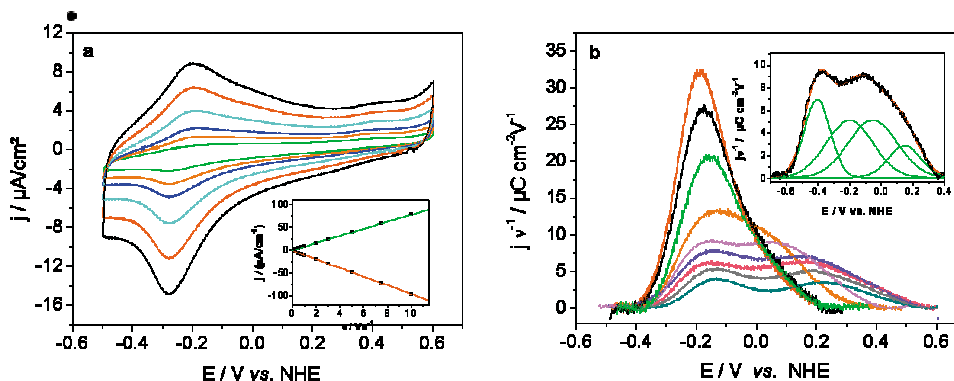


FIG. 5. Cyclic voltammograms of CcO with the his tag attached to SU II under strictly anaerobic conditions. (a) Scan rates between 0.1 and  $1 \text{ V s}^{-1}$ ,  $0.01 \text{ V s}^{-1}$  (green),  $0.02 \text{ V s}^{-1}$  (orange),  $0.03 \text{ V s}^{-1}$  (dark blue),  $0.05 \text{ V s}^{-1}$  (light blue),  $0.075 \text{ V s}^{-1}$  (red), and  $0.1 \text{ V s}^{-1}$  (black). Inset: Base-line-corrected current density plotted as a function of scan rate, reductive branch (red), oxidative branch (green). (b) Oxidative branches (base-line-corrected) of CVs at scan rates between 1 and  $600 \text{ V s}^{-1}$  (current densities normalized by the scan rate,  $\cong 1 \text{ V s}^{-1}$ )  $1 \text{ V s}^{-1}$  (red),  $3 \text{ V s}^{-1}$  (black),  $7.5 \text{ V s}^{-1}$  (green),  $20 \text{ V s}^{-1}$  (orange),  $40 \text{ V s}^{-1}$  (pink),  $300 \text{ V s}^{-1}$  (blue),  $400 \text{ V s}^{-1}$  (violet),  $500 \text{ V s}^{-1}$  (gray), and  $600 \text{ V s}^{-1}$  (light blue). Inset: example of a deconvolution into four Gaussian components.

Cu centers are not visible. Evidence that ET to the hemes indeed occurs via  $\text{Cu}_A$  as described in previous studies<sup>16</sup> was derived from potential-controlled SEIRAS performed on

CcO immobilized in the same orientation in a ptBLM.<sup>20</sup> These measurements make use of amide I bands of the protein environment assigned to specific redox states of  $\text{Cu}_A$ .<sup>21</sup> These results, taken together with the Raman spectra, indicate that the electrochemical reduction peak is in fact due to direct ET to  $\text{Cu}_A$  and further on to the heme centers.

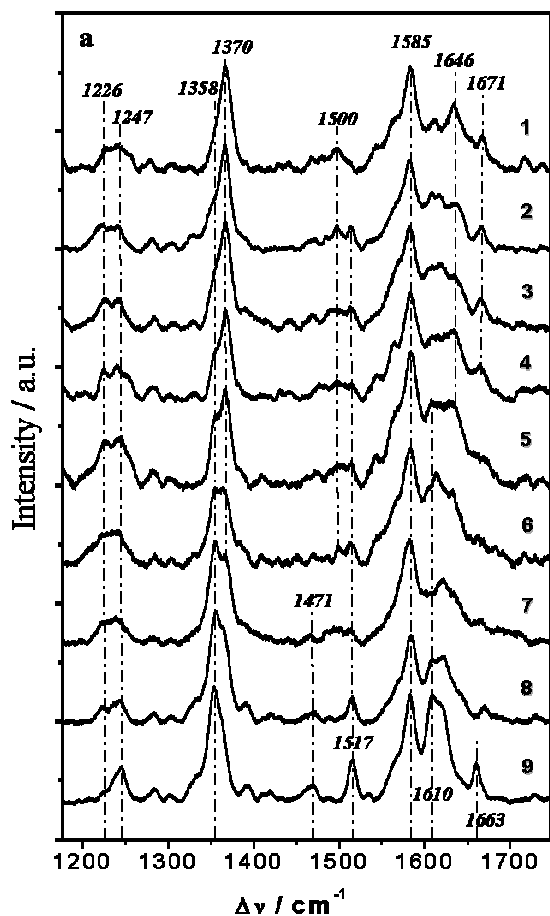


FIG. 6. SERR spectra of CcO at different potentials applied across the biomimetic protein-membrane architecture immersed in buffer solution (a) with the his tag on SU II at (1)  $-150 \text{ mV}$ , (2)  $-175 \text{ mV}$ , (3)  $-200 \text{ mV}$ , (4)  $-225 \text{ mV}$ , (5)  $-250 \text{ mV}$ , (6)  $-275 \text{ mV}$ , (7)  $-300 \text{ mV}$ , (8)  $-325 \text{ mV}$ , and (9)  $-350 \text{ mV}$ .

## V. KINETICS OF ELECTRON TRANSFER

While slow scan rate CV is sufficient to obtain basic ET mechanistic information, scan rates larger than  $1 \text{ V s}^{-1}$  must be utilized to extract kinetic information [Fig. 5(b)]. Under anaerobic conditions, the redox currents display single slightly asymmetric peaks up to a scan rate of  $\sim 1 \text{ V s}^{-1}$  [cf. Fig. 5(a)], indicating the contributions from multiple redox centers. At scan rates above  $1 \text{ V s}^{-1}$ , the capacitive current-corrected peaks become more asymmetric; a second maximum gradually appears as the scan rate exceeds  $20 \text{ V s}^{-1}$  [Fig. 5(b)]. Complex voltammograms of multi-redox-site proteins were previously deconvoluted into a number of Gaussian components with the area of each peak corresponding to the number of electrons transferred in each step.<sup>22</sup> Accordingly, the curves shown in Fig. 5(b) were found to require four Gaussian components to adequately describe the system. However, due to the strong overlap, the peak areas are not evenly distributed, particularly regarding the last component. This is assumed to be caused by the strong coupling of the ET occurring sequentially through the four redox centers  $\text{Cu}_A$ , heme a, heme a, and  $\text{Cu}_B$  in the enzyme [Fig. 5(b), inset], not observed in other enzymes.<sup>23</sup>

Established procedures<sup>23</sup> were used to obtain kinetic rate constants by plotting the peak potentials versus scan rate in a logarithmic scale to yield a “trumpet” plot (Fig. 7).<sup>24</sup> This plot was analyzed by means of the algorithm described by Jeuken *et al.*<sup>25</sup> with the simplifying assumption of an individual one-step ET to each redox center. Because ET between redox centers in CcO occurs sequentially, the values of  $k_0$  for redox centers 2–4 are approximations of lumped rate constants to heme a, heme a<sub>3</sub>, and  $\text{Cu}_B$  through the ET chain.

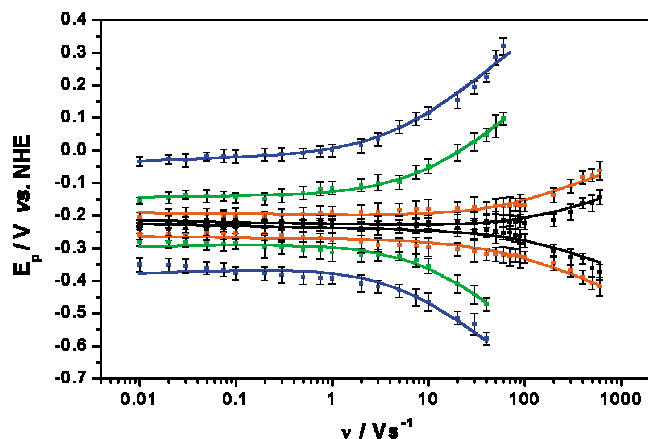


FIG. 7. Peak potentials as a function of scan rate (trumpet plots) of the four redox centers. Peak potentials are obtained by deconvolution of CVs into Gaussian components of oxidation and reduction branches of CcO with the his tag attached to SU II under anaerobic conditions [cf. Fig. 5(b)] for redox centers 1 ( $\text{Cu}_A$ ) (black), 2 (red), 3 (green), and 4 (blue). The error bars represent ranges resulting from the deconvolution procedure.

Values for the rate constant  $k_0$  and the apparent standard potential  $E_{\text{app}}^0$  thus obtained are shown in Table II. However,  $k_0$  for redox center 1 is attributed to ET to  $\text{Cu}_A$ . Hence, it is clear that ET to the subsequent redox centers is not restricted or rate limited by the electrochemical ET to  $\text{Cu}_A$ . Therefore, the measurements in the ptBLM yield results of biological relevance.

## VI. PROTON TRANSPORT COUPLED TO ELECTRON TRANSFER

To investigate the enzyme undergoing catalytic turnover, *aerobic* conditions were used. The CV of CcO with the cytochrome *c* binding side oriented toward the electrode showed two cathodic peaks (Fig. 8, black curve). The first peak at  $-202 \pm 5$  mV, attributed to reduction in the four redox centers of CcO, showed a significant amplification in the current density compared to the peak under anaerobic conditions (Fig. 8, red curve). This is a clear indication of the catalytic turnover of the enzyme. Electrons transferred from the electrode to the redox centers of CcO are irreversibly transferred to oxygen, leading to a continuous electron transfer.<sup>13</sup> The current density ( $35 \mu\text{A cm}^{-2}$ ) of this peak is

TABLE II. Data obtained from CcO from *Rhodobacter sphaeroides* engineered with the his tag attached to SU II. Apparent standard potentials  $E_{\text{app}}^0$  and rate constants  $k_0$  are obtained from CV of CcO under anaerobic conditions. The errors represent ranges resulting from experimental errors, the deconvolution procedure, and the fit routine applied to the trumpet plot for four data sets of the same enzyme preparation.

Redox center	$E_{\text{app}}^0$ (mV)	$k_0$ ( $\text{s}^{-1}$ )
1 (black) $\triangle \text{Cu}_A$	$-231 \pm 8$	$4130 \pm 390$
2 (red)	$-234 \pm 7$	$1650 \pm 170$
3 (green)	$-211 \pm 6$	$68 \pm 8$
4 (blue)	$-183 \pm 7$	$11 \pm 2$

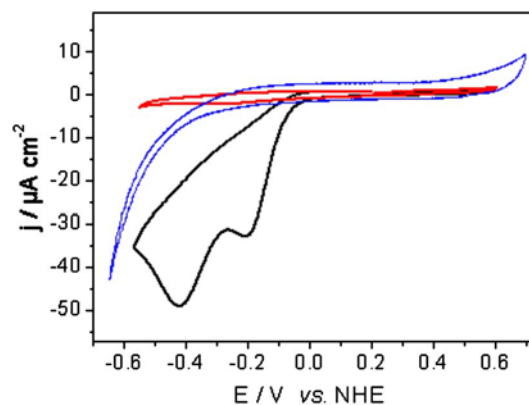


FIG. 8. Voltammograms of CcO with the his tag attached to SU II under aerobic and anaerobic conditions. Cyclic voltammograms are at a scan rate of  $0.01 \text{ V s}^{-1}$ : anaerobic (red), aerobic (black), and CcO with the his tag on SU I (blue).

considerably larger than the one measured previously with the help of soluble substrates of membrane proteins immobilized in a tBLM ( $\leq 0.6 \mu\text{A cm}^{-2}$ ),<sup>23,25</sup> indicating a comparatively high activity of the CcO embedded in the ptBLM.

As a consequence of catalytic turnover of the CcO in the orientation with the his tag attached to SU II, protons are pumped from the bulk solution into the interstitial space between the electrode and the ptBLM. Due to its small volume, around  $0.2 \text{ nl/cm}^2$ , as deduced from the length of the chelator molecules, this interstitial space is thereby highly acidified (as low as  $\text{pH } 2$ , see supplementary information in Ref. 13). These protons are electrochemically reduced to  $\text{H}_2$ , giving rise to the second peak at  $-422 \pm 6$  mV [Fig. 5(a), black curve]. The absence of direct ET and the  $\text{H}^+$  reduction peak in the inverted orientation (Fig. 8, blue curve) further confirms the orientation dependence of direct electron transfer as well as transmembrane proton transport.

## VII. DISCUSSION

These results underline the consideration of the ptBLM as an alternative to hitherto developed biomimetic membranes. Contrary to all the other supported membrane systems including the tethered ones, the ptBLMs are focused on the transmembrane protein rather than on the lipid. The advantage apart from the orientational control is the high surface density of protein molecules. This opens the way to the simultaneous application of vibrational spectroscopy such as Raman and Fourier transform infrared with electrochemistry. High packing densities of proteins can be found in biological systems such as inner mitochondrial membranes, thylacoid, or purple membranes. Mitochondrial membranes, for example, consist of 70% proteins. Packing densities of ptBLMs were optimized by varying the surface concentration of the chelator molecules<sup>16</sup> or in the case of fluorescence spectroscopy, by mixing fluorescent with nonfluorescent proteins. The small submembrane space provided by the chelator molecules (see above) also has a counterpart in biology, namely, the small inner volume of the organelles active in biological

energy conversion such as mitochondria and thylacoids. The small volumes do not seem to impair the protein's ability to actively transport protons across the membrane as long as these volumes are determined by the dimension of the proteins themselves as in the case of the ptBLM. The absence of fluidity also does not seem affect their function, provided the packing density is not too high.<sup>15</sup> A true advantage is the direct accessibility of Faradaic processes such as ET and proton transfer by dc measurements. Impedance spectroscopy is usually not designed to discriminate between Faradaic and non-Faradaic currents. The most direct way to rate constants of a redox-active protein is the bioelectronic coupling to an electrode.

Bioelectronic coupling of a multi-redox-site membrane protein in a functionally active form was verified using CcO as an example.<sup>13–15</sup> This is clearly demonstrated by electrochemical and potential-controlled SERRS experiments. Direct ET to the enzyme is very specifically controlled by the orientation of the CcO immobilized on the surface. Electrons are transferred but only when the CcO is immobilized with the cytochrome c binding side directed toward the electrode, suggesting that the primary electron acceptor is Cu<sub>A</sub>, as in other biochemical assays. Electron transfer appears to be facilitated by the Ni<sup>1+/2+</sup> complex, as deduced from the heterogeneous rate coefficient  $k_0 > 4000 \text{ s}^{-1}$ , which is fast compared to other (soluble) proteins. Previous attempts at coupling proteins to surfaces have yielded  $k_0$  values between 100 and 1600  $\text{s}^{-1}$ .<sup>25–27</sup> Electron injection into the CcO by other methods (see, for example, Ref. 28) is faster, for example, by pulse radiolysis or photochemical excitation.<sup>29,30</sup> In these methods, however, a substrate has to be bound first to the enzyme in a slow diffusion-controlled process before electron injection can be initiated. As a consequence, fast electron injection occurs only once, and a continuous or repetitive process is not possible. By contrast, electrochemical ET is not limited by diffusion. It can be repeatedly performed many times in both the reductive and oxidative directions or alternatively, it can be used to elicit a stationary state of ET. This makes electrochemical ET the method of choice for time-resolved measurements particularly for processes occurring in cycles, e.g., enzymatic cycles. The full enzyme cycle apparently occurs in CcO immobilized in the ptBLM, as is evident from CV scans obtained under aerobic conditions.

ET is often rate limited by protonation reactions; for example, proton uptake of the so-called charge compensating proton of reduced heme a/a<sub>3</sub> occurs in the time scale of 200  $\mu\text{s}$ ,<sup>32</sup> which would yield a first order rate constant of 5000  $\text{s}^{-1}$ . Protonation of the hemes is very likely to occur on electrochemical reduction in the CcO, which would account for an overall  $k_0 > 4000 \text{ s}^{-1}$ . Rates of transitions between other states in the enzyme cycle, e.g., transitions between the states labeled *P* and *F*, or *F* and *O* are considerably slower (in the millisecond time scale).<sup>32</sup> It is thus concluded that the bioelectronic approach is designed to perform kinetic measurements of biological relevance.

Regarding mechanistic details, first insights into the performance of the electrochemical method have been gained by comparative measurements under aerobic and anaerobic conditions. Proton transfer into the interstitial space underneath the membrane only occurs in the presence of oxygen. This observation supports the proposed mechanism of proton pumping, in conjunction with the transition from states *O* to *E*, which requires a preceding full turnover (or an activated state *O<sub>H</sub>*).<sup>33–35</sup> Other proposals contradict this idea, claiming that the transfer of two electrons from states *O* to *E*, is followed by a proton pumping step even with no preceding turnover of the catalytic cycle.<sup>31,32</sup> The latter hypothesis seems questionable in the light of our findings, which suggest that protons are not released to the submembrane space upon a mere reduction in the hemes, i.e., proton pumping does not occur without oxygen present.<sup>33–35</sup> It should be mentioned, however, that the uptake of protons in the *O* to *E*, transition, (the so-called charge compensating protons<sup>31</sup>) is compatible with our experiments.

The result presented in this work demonstrate that the ptBLM is a promising platform for kinetic and mechanistic studies of a large number of membrane proteins, in particular, redox proteins. Studies of other membrane proteins would certainly also benefit from this strategy, considering that electric fields are often a controlling parameter, for example, for ion transport through channel proteins. These options are particularly attractive with respect to the combined application of electrochemical and multiple surface-analytical methods, including vibrational spectroscopy.

<sup>1</sup>L. K. Tamm and H. M. McConnell, *Biophys. J.* **47**, 105 (1985).

<sup>2</sup>E. Sackmann and M. Tanaka, *Trends Biotechnol.* **18**, 58 (2000).

<sup>3</sup>J. K. Cullison, F. M. Hawkridge, N. Nakashima, and Sh. Yoshikawa, *Langmuir* **10**, 877 (1994).

<sup>4</sup>R. Guidelli, G. Aloisi, L. Becucci, A. Dolfi, M. R. Moncelli, and F. T. Buoninsegni, *J. Electroanal. Chem.* **504**, 1 (2001).

<sup>5</sup>W. Knoll, K. Morigaki, R. Naumann, B. Sacca, S. Schiller, and E. K. Sinner, in *Ultrathin Electrochemical Chemo- and Biosensors, Technology and Performance*, edited by V. M. Mirsky (Springer-Verlag, Berlin, 2004), p. 239.

<sup>6</sup>M. Tanaka and E. Sackmann, *Nature (London)* **437**, 656 (2005).

<sup>7</sup>E. Sackmann, *Science* **271**, 43 (1996).

<sup>8</sup>H. Hillebrandt, G. Wiegand, M. Tanaka, and E. Sackmann, *Langmuir* **15**, 8451 (1999).

<sup>9</sup>S. M. Schiller, R. Naumann, K. Lovejoy, H. Kunz, and W. Knoll, *Angew. Chem., Int. Ed.* **42**, 208 (2003).

<sup>10</sup>F. Giess, M. G. Friedrich, J. Heberle, R. L. Naumann, and W. Knoll, *Biophys. J.* **87**, 3213 (2004).

<sup>11</sup>K. Ataka, F. Giess, W. Knoll, R. Naumann, S. Haber-Pohlmeier, B. Richter, and J. Heberle, *J. Am. Chem. Soc.* **126**, 16199 (2004).

<sup>12</sup>M. G. Friedrich, M. A. Plum, M. G. Santonicola, V. U. Kirste, W. Knoll, B. Ludwig, and R. L. C. Naumann, *Biophys. J.* (to be published).

<sup>13</sup>M. G. Friedrich, J. W. F. Robertson, D. Walz, W. Knoll, and R. L. C. Naumann, *Biophys. J.* (in press).

<sup>14</sup>M. G. Friedrich, F. Giess, R. Naumann, W. Knoll, K. Ataka, J. Heberle, J. Hrabakova, D. H. Murgida, and P. Hildebrandt, *Chem. Commun. (Cambridge)* **2004**, 2376.

<sup>15</sup>M. G. Friedrich, V. U. Kirste, J. Zhu, R. B. Gennis, W. Knoll, and R. L. C. Naumann, *J. Phys. Chem. B* (in press).

<sup>16</sup>O.-M. H. Richter and B. Ludwig, *Rev. Physiol. Biochem. Pharmacol.* **147**, 47 (2003).

<sup>17</sup>D. M. Mitchell and R. B. Gennis, *FEBS Lett.* **368**, 148 (1995).

<sup>18</sup>S. J. Döpner, B. Hudecek, B. Ludwig, H. Witt, and P. Hildebrandt, *Biochim. Biophys. Acta* **1480**, 57 (2000).

<sup>19</sup>G. E. Heibel, P. Hildebrandt, B. Ludwig, P. Steinrück, T. Soulimane, and

- G. Buse, *Biochemistry* **32**, 10866 (1993).
- <sup>20</sup>Unpublished results.
- <sup>21</sup>E. A. Gorbikova, K. Vuorilehto, M. Wikström, and M. I. Verkhovsky, *Biochemistry* **45**, 5641 (2006).
- <sup>22</sup>F. A. Armstrong, *J. Chem. Soc. Dalton Trans.* 661 (2002).
- <sup>23</sup>L. J. C. Jeuken, J. P. McEvoy, and F. A. Armstrong, *J. Phys. Chem. B* **106**, 2304 (2002).
- <sup>24</sup>E. Laviron, *J. Electroanal. Chem. Interfacial Electrochem.* **101**, 19 (1979).
- <sup>25</sup>L. J. C. Jeuken, S. D. Connell, P. J. F. Henderson, R. B. Gennis, S. D. Evans, and R. J. Bushby, *J. Am. Chem. Soc.* **128**, 1711 (2006).
- <sup>26</sup>L. J. C. Jeuken, *Biochim. Biophys. Acta* **1604**, 67 (2003).
- <sup>27</sup>J. Hirst, J. L. C. Duff, G. N. L. Jameson, M. A. Kemper, B. K. Burgess, and F. A. Armstrong, *J. Am. Chem. Soc.* **120**, 7085 (1998).
- <sup>28</sup>J. R. Winkler, B. G. Malmström, and H. B. Gray, *Biophys. Chem.* **54**, 199 (1995).
- <sup>29</sup>K. Kobayashi, H. Une, and K. Hayashi, *J. Biol. Chem.* **264**, 7976 (1989).
- <sup>30</sup>T. Nilsson, *Proc. Natl. Acad. Sci. U.S.A.* **89**, 6497 (1992).
- <sup>31</sup>M. Ruitenber, A. Kannt, E. Bamberg, K. Fendler, and H. Michel, *Nature (London)* **417**, 99 (2002).
- <sup>32</sup>H. Michel, *Biochemistry* **38**, 15129 (1999).
- <sup>33</sup>M. I. Verkhovsky, A. Jasaitis, M. L. Verkhovskaya, J. E. Morgan, and M. Wikström, *Nature (London)* **400**, 480 (1999).
- <sup>34</sup>M. I. Verkhovsky, I. Belevich, D. A. Bloch, and M. Wikström, *Biochim. Biophys. Acta* **1757**, 401 (2006).
- <sup>35</sup>K. Faxen, G. Gilderson, P. Adelroth, and P. Brzezinski, *Nature (London)* **437**, 286 (2005).